A Density Functional Theory Study of Catalytic *trans*-Esterification by *tert*-Butoxide MgAl Anionic Clays

H. Chris Greenwell,*,† Stephen Stackhouse,‡ Peter V. Coveney,*,‡ and William Jones†

Department of Chemistry, University of Cambridge, Lensfield Road, Cambridge, U.K. CB2 1EW, and Centre for Computational Science, Department of Chemistry, University College London, 20 Gordon Street, London, U. K. WC1H 0AJ

Received: December 9, 2002; In Final Form: January 30, 2003

We use ab initio plane-wave density functional theory (PW-DFT) to investigate, for the first time, prospective solid base catalytic pathways within anionic clays. MgAl-layered double hydroxides (LDHs) intercalated with *tert*-butoxide anions are known to be excellent solid base catalysts for a wide range of reactions. PW-DFT is used here to investigate a reaction mechanism proposed by Choudary et al. (Choudary, B. M.; Kantam, M. L.; Reddy, C. V.; Aranganathan, S.; Santhi, P. L.; Figueras, F. *J. Mol. Catal. A Chem.* **2000**, *159,* 411−416) for the LDH-*t*-butoxide-catalyzed transesterification reaction of methylacetoacetate with prop-2-en-1-ol. We have studied a variety of plausible orientations and interactions of molecules within this host−guest system. Our study leads to our postulating an alternative mechanism, which is consistent with both simulation and experiment. Regeneration of the catalyst requires the presence of interlayer water and indicates that the active catalyst is a hydroxide charge balanced LDH, with neutral *tert*-butyl alcohol molecules present in the LDH host interlayer. The presence of interlayer water and/or hydroxide anions, coupled with the variable interlayer spacing of LDHs, facilitates interactions between the LDH host and the guest species. The hydrophobic nature of the interlayer region in organo-LDHs results in organic substrate molecules with polar functional groups being intercalated in a preferred orientation, facilitating reactions and promoting catalytic behavior. Our study illustrates the viability of the PW-DFT method for the study of these systems.

1. Introduction

Layered double hydroxides (LDHs) are the anionic counterparts to the abundant cationic clay mineral family of materials. A large variety of inorganic and/or organic anionic guests may be intercalated within the gallery region of the LDH host. LDHs exist both as naturally occurring minerals and as an increasing variety of synthetic analogues produced in the laboratory.[1−3] LDHs are of increasing commercial interest due to their potential application as nanocomposites,[4] drug delivery reagents,[5,6] catalysts,[7,8] and adsorbents.[9]

Structurally, layered double hydroxides may be considered as analogous to the magnesium hydroxide mineral brucite. Brucite consists of Mg^{2+} ions octahedrally coordinated by hydroxyl groups. The octahedra share edges in such a way that infinite sheets of mono-octahedra thickness are formed in the *ab* crystallographic plane. These sheets stack in the *c* direction, held together by hydrogen bonding between the hydroxyl groups on adjacent sheets. In the largest group of LDHs some of the Mg^{2+} is substituted by a M^{3+} species, for example, Al^{3+}, Fe^{3+},[10] or Ga^{3+}.[11] The resultant structure consists of layers bearing a net positive charge, which is compensated by the introduction of anions in the interlayer (gallery) region between the layers. Invariably, during synthesis, some water is associated with the anions and also taken into the interlayer. A balance of repulsive and attractive Coulombic forces, hydrogen bonding, size of anion and hydration state dictate the interlayer separation. Other varieties of LDHs exist where the M^{2+} species is not Mg, giving rise to the family of compounds of the general structure $M^{2+}_{1-x}M^{3+}_{x}(OH)_2A^{x-}\cdot nH_2O$.

The use of LDHs as heterogeneous catalysts has been well-documented.[12] The predominant catalytic application of LDHs is their utilization as precursors that are calcined to form basic mixed metal oxide catalysts.[13−15] Suitably modified noncalcined LDHs also prove to be efficient catalysts for a multitude of reactions.[7,16−21] The use of solid base catalysts is not nearly as extensive as that of cationic clay minerals and zeolites for solid acid catalysis.

The characterization of LDHs is problematic due to the invariably polycrystalline nature of the material, coupled with the dynamic nature of, and disorder present within, the interlayer region, particularly in the case of organo-LDHs. Only the structure of naturally occurring hydrotalcite has been solved by single-crystal diffraction methods.[22] Refinement of powder patterns has only been achieved in instances where small inorganic guests are intercalated.[23] Other methods of characterization, such as FTIR and EXAFS, yield limited information regarding the interlayer arrangement.

Computational methods have been applied to elucidate the nature of the interlayer arrangement within LDHs. Until very recently, all of these studies have been carried out using parametrized force field based calculations. Both inorganic[24,25] and organic[26−28] interlayer species have been investigated, mainly within MgAl LDHs. The large size of model required to meaningfully simulate the structure and chemistry of LDHs has largely prevented the use of computationally intensive ab initio methods to study these materials. Recently, however,

* To whom correspondence should be addressed. (H. Chris Greenwell) E-mail: hcg21@cam.ac.uk. (Peter V. Coveney) E-mail: P.V.Coveney@ucl.ac.uk.

† University of Cambridge.

‡ Centre for Computational Science.

10.1021/jp027663i CCC: $25.00
Published on Web 03/20/2003

Trave et al. have described the simulation of simple, anhydrous inorganic LDHs using a variable-cell first-principles molecular dynamics (FPMD) approach.[29] The authors examined certain structure−property relationships of MgAl-hydroxide and -chloride LDHs, and report good correlation with experimental results.[29] With the advent of increasingly powerful parallel computers the development of ab initio calculations for describing condensed matter is a burgeoning area and others have described the computational techniques utilized here in more rigorous detail in earlier papers. Notably, Stackhouse et al. have recently applied calculations of the type used here to in-situ polymerization reactions in cationic clays.[30]

The application of density functional theory to the simulation of condensed matter systems is a well-established field. A detailed account of the DFT plane-wave, pseudopotential supercell method, as used here, has been given by Payne et al.[31] Layered solids such as LDHs are particularly suited to plane-wave supercell methods, having none of the problems associated with surfaces where portraying the underlying bulk results in further approximations.[32]

In this paper we use ab initio density functional theory (DFT) molecular dynamics and energy minimization routines to examine the transesterification reactions of MgAl *tert*-butoxide LDH catalysts.[33] In the next section we summarize the experimental work of Choudary et al. for the catalyst synthesis and reactions.[33] In section 3 we describe the methodology employed for the ab initio study of the reaction mechanism. Initially the proposed reaction mechanism of Choudary et al. was investigated,[33] and the limitations of this mechanism are discussed in section 4. As a result of these limitations we propose in section 5 an alternative modified mechanism, which enables us to simulate the whole catalytic cycle. Section 6 presents the conclusions from this work.

2. MgAl *t*-butoxide LDH Catalyst

The MgAl *t*-butoxide catalyst used by Choudary et al. was prepared via a nitrate-intercalated MgAl LDH synthesized by the conventional coprecipitation route, which was then exchanged with *t*-butoxide to generate the basic catalyst.[33,34] During coprecipitation synthesis of the nitrate MgAl LDH some water is invariably intercalated into the interlayer region of the LDH as it forms. Typically the Al:water content is 1:2 though may reach 1:6, depending upon the extent of drying, Mg/Al ratio and other factors.[35]

Transesterification involves the reaction of an alcohol with an ester resulting in the exchange of the more labile ester alkoxy substituent for the alcohol.[36] Conventionally either soluble base[37,38] or acid catalysts[39] are used to mediate these reactions, but these reagents present a problem for bulk synthesis due to the problem of catalyst separation and the environmental impact of a highly basic or acidic effluent stream. The transesterification reaction is industrially important for the production of paint additives, pheromones, and other natural product synthesis.[36] Choudhary et al.[33] have shown that excellent selectivity and conversion may be achieved using the modified MgAl LDH catalyst for a range of normal and β-keto-esters with numerous types of alcohols and amines.

In the work of Choudary et al., the reactants and catalyst were dissolved in toluene solvent at 363 K and the reaction monitored by thin-layer chromatography. High yields were reported across the wide variety of substrates investigated.[33] Choudary et al. suggest a simple model catalytic cycle based upon the classic base catalyzed reaction mechanism,[37] as illustrated in Figure 1.[33] Comparison with other LDH catalysts

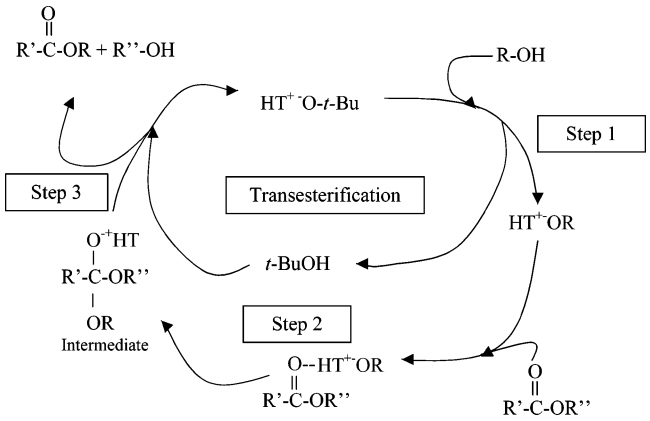

Figure 1. Scheme to show Choudary et al.'s proposed mechanism for catalytic process, after Choudary et al.[33] In our simulations the mechanism fails at Stage 3, with no catalyst regeneration observed. HT refers to hydrotalcite, the naturally occurring mineral MgAl-carbonate LDH (LDHs are sometimes denoted HTLCs, hydrotalcite like compounds). In the diagram R denotes CH_3 or C_2H_5; R′ is a normal or β-ketoester; R″ maybe a primary, secondary, unsaturated, allylic, cyclic, hindered alcohol, or amine.

showed that the *t*-butoxide MgAl catalyst was more efficient than a calcined-rehydrated LDH catalyst where the basic species is the hydroxide anion, which was in turn more efficient than a calcined MgAl LDH where the basic sites are oxygen.[33] The calcined-rehydrated LDH catalyst has been shown to be less basic than the calcined mixed metal oxide catalyst and its increased activity is attributed to the presence of OH^-.[33,40] Further work has ascertained that the *t*-butoxide must be an integral part of the LDH catalyst, rather than simply adsorbed.[17,34] In this paper we take Choudary's simple model cycle and simulate the key processes occurring at each step.[33]

3. Simulation Method

In this section we describe the route taken in setting up the simulations. Details of the energy minimization (optimization) method are given, along with the models used to validate the selection of the exchange-correlation functional. A description of the computers used is also provided.

Our simulation study consisted of several steps: (i) selection of a suitable exchange-correlation functional, (ii) postulation of a series of discrete steps by which the reaction may occur, (iii) model construction, and (iv) simulation of the chosen steps.

3.1. Geometry Optimization. Plane-wave DFT calculations were performed using the CASTEP code.[31,44] For both geometry optimization and molecular dynamics simulations the kinetic energy cutoff was set at 340 eV, just 1 k-point was allowed in the Brillouin zone located at (0, 0, 0) and the ultrasoft pseudopotentials of Vanderbilt were employed.[45] The Broyden−Fletcher−Goldfarb−Shanno (BFGS) algorithm was used to search the potential energy surface during optimization. An external hydrostatic pressure of 0.0001Gpa was applied.

3.2. Molecular Dynamics. Molecular dynamics simulations were performed within the canonical (NVT) ensemble with a thermostat time constant of 0.01ps. The time step used was 1.0fs. The temperature was set at the experimental value of 363 K[33] and all atoms were assigned initial velocities corresponding to thermal motion at this temperature.

3.3. Selection of Suitable Functional. Four exchange-correlation functionals are available within the CASTEP code: LDA,[46] PW91,[47] PBE,[48] and RPBE.[49] To select the most suitable for simulation of LDH's a series of preliminary geometry optimizations were performed where each functional was used

TABLE 1: Calculated and Experimental Cell Parameters of Optimized Structures

		selected exchange −correlation functional				
system	parameter	LDA	PW91	PBE	RPBE	exptl
Brucite[41]	*a*/Å	3.1352	3.2180	3.2242	3.2689	3.1420
	b/Å	3.1299	3.2071	3.2083	3.2546	3.1420
	c/Å	4.7204	4.8155	4.8228	4.8173	4.7660
	α/deg	89.9982	89.9397	89.4832	89.7717	90.0000
	β/deg	89.9929	90.0946	90.7415	90.5325	90.0000
	γ/deg	119.8269	120.3995	120.4256	120.6549	120.0000
	volume/Å^3	40.1856	42.8660	43.0144	44.0869	40.7471
Gibbsite[42]	*a*/Å	8.6117	8.6885	8.6941	8.7526	8.6840
	b/Å	4.9461	5.0458	5.0515	5.0874	5.0780
	c/Å	9.3079	9.5276	9.5430	9.6391	9.3360
	α/deg	90.0180	90.0977	90.1235	90.2608	90.0000
	β/deg	93.9749	93.8139	93.9057	93.7671	94.5400
	γ/deg	89.9899	89.9831	90.0037	89.9726	90.0000
	volume/Å^3	395.513	416.767	418.141	428.282	410.401
Magnesium *o*-chloro cinnamate[43]	*a*/Å	5.6426	5.8421	5.8635	5.9376	5.7790
	b/Å	5.1879	5.4050	5.3998	5.4784	5.3000
	c/Å	35.8009	35.8901	35.8634	35.9554	35.8110
	α/deg	89.9418	89.9062	90.1902	90.3510	90.0000
	β/deg	94.4668	95.4417	95.7702	95.9357	95.0600
	γ/deg	89.9724	90.1952	90.1201	89.9700	90.0000
	volume/Å^3	1044.83	1128.14	1129.70	1163.29	1092.57

to minimize the total energy of a unit cell of each of several layered materials for which structures have been solved by single-crystal X-ray diffraction: brucite,[41] gibbsite,[42] and hexa-aqua magnesium *p*-chlorocinnamate[43] (Table 1).

Comparison of the optimized structures with experimental data showed that in general LDA overestimated bonding, leading to a commensurate reduction in cell parameters of between 1.5 and 4.5%. The PBE functional is a more robust development of the PW91 functional and was observed to result in overestimation of the cell volume by 2−5%. These results are in agreement with those reported Gale et al. from their ab initio study of the aluminum tri-hydroxide polymorphs, gibbsite and bayerite.[50] The RPBE potential was found to typically overestimate cell parameters with an increased volume of up to 8%. In fact, the RPBE functional is just a revision of the PBE functional developed to give improved adsorption energies of molecules on metallic surfaces.

We decided, from the validation described here and prior work, to use the PBE potential to describe the exchange correlation energy term.

3.4. Model Systems. The model MgAl LDH layer was constructed using the atomic coordinates of the naturally occurring mineral brucite.[41] A simple supercell was constructed consisting of 3 × 4 × 1 brucite unit cells. One Mg atom was substituted for an Al atom and, for simplicity, only one interlayer region modeled. Two interlayer spacings were initially investigated, 16 and 14 Å. These distances were chosen on the basis of values observed experimentally for similar organo-LDHs since no experimental data is available for the catalytic system investigated. Initial trials showed that models with an interlayer spacing of 14 Å frequently failed to converge during optimization, so the 16 Å cell was utilized throughout unless otherwise stated.

The solvent used by Choudary et al. in the experiment was toluene,[33] and since this was deemed to play no part in the reaction, this was omitted for the simulations, i.e., simulations were treated as being in vacuo. Though water is invariably present in LDHs, being incorporated into the interlayer region during synthesis, none was initially included in the simulations as experimental conditions preclude its presence.

The cell parameters and selected bond lengths and angles for the optimized LDH layer are given in Table 2 (by optimized we mean minimized with respect to potential energy). A marked contraction of the Al−O bond lengths and a concomitant increase of the Mg−OAl bond lengths were observed. The layer became compressed along the *c* axes with O−Mg−O angles adjacent to Al decreasing by approximately 8−9°. The *ab*-AlO−H angle decreased slightly to ca. 87° resulting in the hydrogens slightly pointing inward toward the center of the Al octahedral face. Optimization of the single organic molecules by use of a plane-wave basis set may seem implausible but previous research has shown that a supercell approach, such as used here, yields results of comparable accuracy to Hartree−Fock (HF) type calculations.[52] The organic molecule was placed in a supercell with at least 10 Å vacuum gap between its repeat image in the adjacent supercell. All cell parameters were fixed during the optimization process, and no external hydrostatic pressure was introduced, i.e., the molecules were optimized in vacuo. It was found that increasing either the kinetic energy cutoff for the plane wave basis set or the unit-cell size had little effect on the optimized energy or structure of a *tert*-butyl alcohol molecule (Table 3). In the case of anionic species, for example

TABLE 2: Selected Calculated Unit Cell and Bond Parameters for Simulated LDH Layers

parameter	optimized LDH layer	LDH catalyst (section 4.1)	step 1 in Figure 1 (section 4.2)	step 2 in Figure 1 (section 4.3)
a	9.512 Å	9.524 Å	9.584 Å	9.569 Å
b	12.620 Å	12.626 Å	12.715 Å	12.692 Å
α	90.06°	90.05°	90.45°	90.04°
β	90.00°	90.09°	89.88°	90.47°
AlO−H13	0.969 Å	1.009 Å	0.975 Å	0.984 Å
AlO−H30	0.969 Å	1.003 Å	0.975 Å	0.993 Å
AlO−H40	0.969 Å	1.009 Å	0.982 Å	0.989 Å
Al−O1	1.890 Å	1.911 Å	1.903 Å	1.902 Å
Al−O4	1.902 Å	1.934 Å	1.935 Å	1.926 Å
Al−O7	1.892 Å	1.904 Å	1.913 Å	1.910 Å
Al···Mg (mean)	3.169 Å	3.138 Å	3.175 Å	3.162 Å
ab-AlO−H13	87.52°	70.90°	82.86°	76.34°
ab-AlO−H30	87.79°	72.38°	81.34°	73.70°
ab-AlO−H40	88.34°	69.82°	72.41°	74.34°
Mg16−O12Al	2.193 Å	2.126 Å	2.189 Å	2.140 Å
Mg46−O42	2.105 Å	2.105 Å	2.103 Å	2.101 Å
Mg46−O47	2.133 Å	2.141 Å	2.137 Å	2.132 Å
Mg46−O52	2.099 Å	2.112 Å	2.075 Å	2.098 Å
ab-MgO−H20	88.02°	85.45°	86.63°	86.81°
ab-MgO−H43	88.09°	86.02°	88.15°	86.69°
ab-MgO−H3	88.63°	84.05°	72.91°	72.91°

TABLE 3: Selected Calculated and Experimental Bond Parameters of *tert*-Butyl Alcohol

	bond (length, Å; angle, deg)						
t-butanol	O−H	C−O	C−C	C−H	C−C−C	O−C−C	energy (eV)
cutoff 340 eV	0.974	1.439	1.511−1.522	1.092	110.4	105.1	−1222.9965
cutoff 380 eV	0.976	1.439	1.514−1.519	1.092	110.7	104.9	−1222.9948
unit cell increased	0.974	1.440	1.514−1.520	1.092	111.0	105.3	−1222.9496
exptl[51]		1.459	1.536−1.645		110.8	106.2	

TABLE 4: Selected Calculated and Experimental (crystal) Bond Parameters for *t*-butoxide

	bond parameter			
t-butoxide	C−O/Å	C−C/Å	C−H/Å	∠C−C−C/°
calcd	1.347	1.550	1.099	107.9
zinc salt[53a]	1.397	1.523	0.960	108.4
zinc salt[53b]	1.405	1.514	0.960	108.8
potassium salt[54c]	1.462	1.526		110.2
sodium salt[55d]	1.453	1.546		108.0

[a] Dipotassium bis((2-*t*-butoxo)-di-*t*-butoxy-zinc). [b] Disodium bis((2-*t*-butoxo)-di-*t*-butoxy-zinc). [c] Dotetraconta-potassium dodecakis (1-*tert*-butyl-2-methyl-1,3,2-diazaborolyl)octadeca-kis(butoxy)hexakis(dimethylsilanediolate) tetrahydrofuran solvate. [d] Sodium *t*-butoxide.

t-butoxide, the calculated bond parameters were compared with those from crystal structures of various salts containing the anion (Table 4).

Each simulation supercell consisted of the optimized LDH layer model and the relevant optimized organic molecules placed in the interlayer region. Bulk structure was represented by utilizing periodic boundary conditions, i.e., the supercell was considered to be replicated infinitely in *a*, *b*, and *c* directions. Each model system was then optimized. If the desired reaction failed to occur through simple optimization, temperature effects were then included, i.e., molecular dynamics simulations at the experimental conditions of 363 K were carried out.

3.5. Computational Details. Calculations were carried out on 16 processors of the 64 CPU SGI Origin 2000 machine (300 MHz processor speed) at the Cambridge-Cranfield High Performance Computing Facility (HPCF) at Cambridge. Some of the initial optimizations were completed on 4 processors of a 16 processor (400 MHz processor speed) SGI Onyx2 machine at Queen Mary, University of London.

4. Results and Discussion: MgAl *t*-Butoxide Catalyst

In this section we present the results from our simulation studies of the mechanism proposed by Choudary et al.[33] The computations are discussed in relation to the experimental procedures and the implication of our findings are analyzed insofar as they pertain to the catalytic activity of the material. The starting point is the study of the interlayer arrangement and interactions of the MgAl *t*-butoxide LDH catalyst, followed by an analysis of the simulation of the postulated steps of the catalytic cycle identified earlier (section 2). We go on to outline the failings of the proposed mechanism of Choudary et al. and, in section 5, outline a mechanism by which the catalytic process may proceed.

4.1. Optimized *t*-Butoxide LDH Catalyst. Here we describe the procedure we used to model the structure of the MgAl LDH-*t*-butoxide catalyst, the starting point for the catalytic cycle given in Figure 1. Various possible binding sites were identified on the optimized LDH sheet where the optimized *t*-butoxide anion might be placed. These were directly above an Al atom, directly above an Mg atom adjacent to Al, directly above a Mg atom adjacent to only Mg atoms, and above the hydroxyl group bridging Mg and Al atoms (Figure 2). The optimized *t*-butoxide

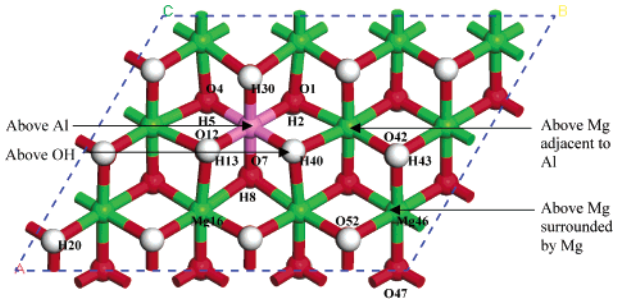

Figure 2. Layer used for simulation shown in *ab* plane with the possible *t*-butoxide/prop-2-en-1-ol binding sites identified. The color scheme used is white for hydrogen, red for oxygen, green for magnesium, purple for aluminum, and the boundary conditions for the periodic supercell are denoted by blue dashed lines.

TABLE 5: Binding Energy for Various Species on LDH Layer

molecule	location on LDH layer (See Figure 2)	binding energy/eV
t-butoxide	above Al atom	−0.4906
t-butoxide	above Mg atom adjacent to Al atom	−0.3841
t-butoxide	above Mg atom adjacent to Mg atoms	−0.0499
t-butoxide	above OH bridging Mg and Al atom	
OH^-	above Al atom	−0.8116
OH^-	above Al atom, *t*-BuOH present	−0.8049
OH^-	above Al atom, prop-2-en-1-ol and 2*t*-BuOH	−0.7812
H_2O	oxygen atom of H_2O above Al atom	−0.3848
NO_3^-	nitrogen atom above Al atom, parallel	+0.9625

molecule was placed in turn 4 Å above each of these possible sites. Each system was then geometry-optimized with respect to potential energy. The binding energy for the *t*-butoxide molecule−LDH interaction was calculated at each possible site using single-point energy calculations of the optimized systems and the results are presented in Table 5.

Those sites directly above LDH layer cations resulted in a tri-axial coordination of the *t*-butoxide oxygen atom via H-bonding to the LDH layer hydroxyl groups, while sites above a hydroxyl group resulted in only one coordinating H-bond. A third type of site where the *t*-butoxide oxygen atom would sit between two hydroxide groups was not investigated. Those sites above the LDH layer cations were found to vary in binding energy in the order: site above Al atom > site above Mg atom adjacent to Al atom > site above Mg atom adjacent to only Mg atoms. The model with the *t*-butoxide at the site above a hydroxyl group failed to converge. The model system with the highest binding energy, and lowest overall energy, was the arrangement with the *t*-butoxide molecule located on the LDH layer above the Al cation. The unit cell, and selected bond, parameters for the LDH layer for this optimized model are given in Table 2.

The *t*-butoxide anion was found to locate in the interlayer above the Al center at a distance of 3.118 Å from the Al atom, triaxially hydrogen bonding (H-bonding) to the three hydroxyl groups coordinated to the Al atom. The H-bonding interactions occur over a distance of between 1.687 and 1.753 Å and result in an increase over the in vacuo C−O^- bond length by 0.044−

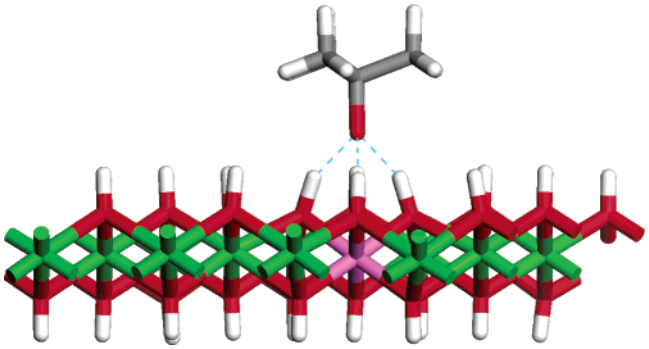

Figure 3. Optimization of *t*-butoxide LDH catalyst showing distortion of AlO−H bonds and H-bonding (dashed lines). The color scheme is as for Figure 2, with gray used for carbon and pale blue dashed lines indicating hydrogen bonding. Periodic boundary conditions are imposed in all three orthogonal space directions, with a vertical interlayer spacing of 16 Å.

1.391 Å. A negligible increase in the C−C−C angle was observed, correlating with the increased C−O^- bond length.

The presence of the *t*-butoxide anion was observed to strongly affect the arrangement of the hydroxyls on the sheet, as illustrated in Figure 3. The hydroxyl groups immediately adjacent to the *t*-butoxide molecule were observed to orient toward the negative O^-, with *ab*-AlO−H angles decreasing by some 17° to approximately 70° and the AlO−H bond length increasing by about 4% due to the strong interaction with the *t*-butoxide anion. No deprotonation of the LDH hydroxyl groups was observed, confirming the strong basic nature of the MgAl layer oxygen atoms. The distance between the Al atom and the six neighboring Mg atoms was found to decrease by about 1% due to the AlO−Mg bonds contracting at the interacting face of the sheet, and lengthening slightly less on the opposite face, resulting in a slight distortion in the layers during optimization. Despite this, a slight increase was noted in the *a* and *b* parameters due to increased compression of the MgAl-hydroxide sheet in the *c* direction. Wang et al, using a classical MD approach, have suggested that the Mg^{2+} ions become displaced in the structure, moving toward one side of the hydroxyl layer.[25] We saw no evidence of this in our model system.

4.2. Deprotonation of Prop-2-en-1-ol by *tert*-Butoxide in the LDH Gallery. This process corresponds to step 1 in the proposed mechanism of Choudary et al. in Figure 1.[33] The optimized *t*-butoxide supercell was taken; the optimized prop-2-en-1-ol molecule was introduced into the interlayer and the energy of the resultant system minimized. To maximize the probability of successful reaction the critical angle and distance between the *t*-butoxide oxygen atom and the acidic proton on prop-2-en-1-ol were kept as close as possible to 180° and 2 Å, respectively. This necessitated raising the *t*-butoxide molecule from the LDH surface slightly.

Deprotonation was observed to occur readily from the prop-2-en-1-ol molecule coordinating with the LDH layer via H-bonding between the prop-2-en-1-ol and a hydroxyl group between two Mg cations (Figure 4a). The H-bond formed was 2.278 Å immediately prior to deprotonation, with the O^- on the *t*-butoxide at a distance of 1.252 Å from the acidic proton. This resulted in a lengthening of the O−H bond to 1.172 Å compared to 0.974 Å in the in vacuo optimized model, and facilitated deprotonation by the *t*-butoxide molecule.

In the optimized structure (Figure 4b) the generated alkoxide (prop-2-en-1-oxide) was H-bonded in a position over a Mg cation adjacent to the Al atom, with two H-bond interactions. These were 1.715 and 2.225 Å long for the MgO−H and the AlO−H donor atoms, respectively.

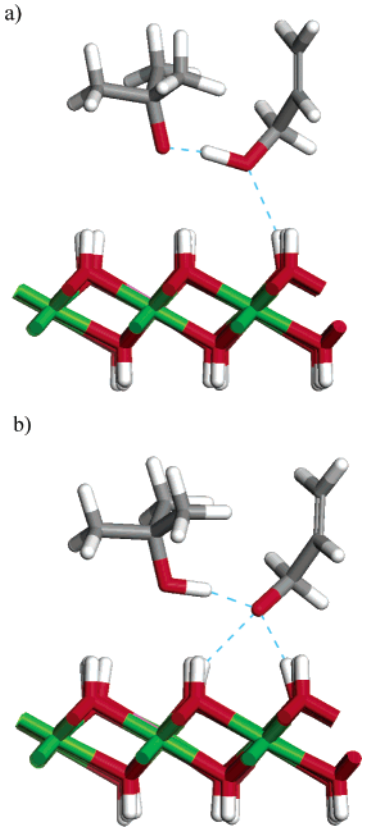

Figure 4. Optimization of step 1. (a) Model just prior to deprotonation and (b) upon convergence of optimization process. The color scheme is the same as that for Figure 2 with gray for carbon, and pale blue dashed lines indicating hydrogen bonds.

The *ab*-M^{x+}O−H angle again decreased sharply to 72.4° where M is Al, and 72.9° where M is Mg (Table 2). The Mg to O^- distance was 3.641 Å at an angle of 73.5° to the *ab* plane. The *tert*-butyl alcohol molecule moved to a distance of 4.053 Å from the Al cation and no longer strongly interacted with the hydroxyl groups coordinated to the Al. This was illustrated by the *ab*-AlO−H angles increasing to 81.33° and 82.86° with bond lengths of 0.975 Å, intermediate between those observed in the optimized layer/*t*-butoxide supercell and those found in the optimized layer without any anions. The *a* and *b* unit cell parameters of 9.584 and 12.715 Å were again larger than those found for both the bare optimized LDH layer and the optimized layer/*t*-butoxide model.

The association of the O^- within the prop-2-en-1-oxide with the LDH layer hydroxyl groups resulted in an increase in the C−O^- bond length to 1.386 Å when compared to 1.340 Å found in the vacuum optimized prop-2-en-1-oxide. There was still H-bonding (1.534 Å) between the prop-2-en-1-oxide and the O−H of *tert*-butyl alcohol (Figure 4b), with the O−H bond at 1.044 Å, some 7% longer than that found in the in vacuo optimized *tert*-butyl alcohol.

4.3. Reaction of Prop-2-en-1-oxide with Methyl Acetoacetate. Choudary et al. have suggested that the driving force for this process is the association of the polarized oxygen of the carbonyl group with the MgAl layer, partially stabilizing the positive charge of the LDH[33] and increasing the reactivity of the deprotonated prop-2-en-1-ol (step 2 in Figure 1).

Initial simulations with the deprotonated prop-2-en-1-ol placed above the Al of the hydroxyl layer, under the assumption that it displaced the *tert*-butyl alcohol from its position, and the methyl acetoacetate placed with the ester carbonyl parallel to the layer and adjacent to a hydroxyl group bridging two

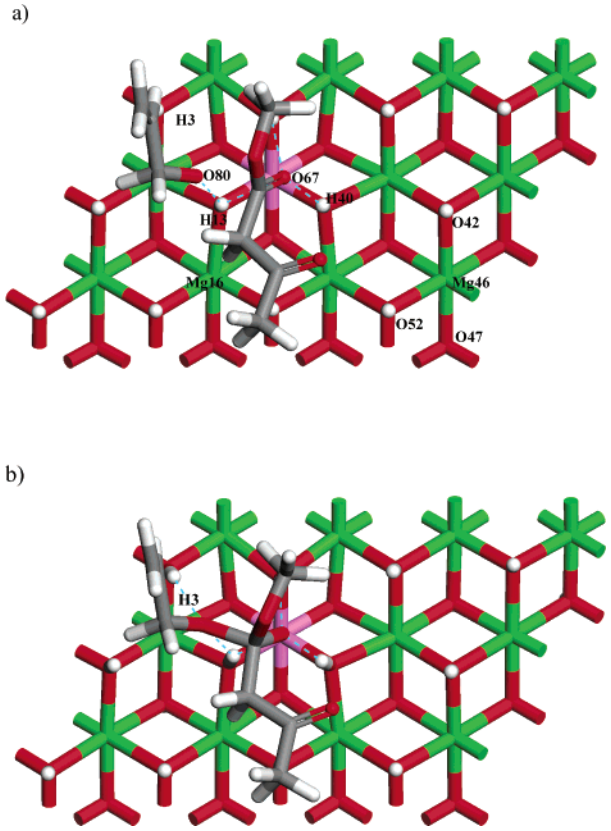

Figure 5. Step 2 optimization, showing (a) model prior to bond formation and (b) model after optimization. The color scheme is the same as that as for Figure 4.

magnesium atoms failed to result in the desired reaction. The two molecules were observed to move apart upon optimization.

Accordingly, a further scenario was investigated with the ester carbonyl oxygen and ester oxygen both parallel to the layer, and sited above the layer Al, with hydrogen bonding of both these groups to hydroxyls attached to the Al. The prop-2-en-1-oxide anion was positioned close to the ester carbonyl carbon atom. This arrangement also failed to result in bond formation.

The simulation where nucleophilic attack occurred involved an arrangement such that the ester carbonyl group was triaxially coordinated to all 3 of the Al-hydroxyl groups, with the deprotonated prop-2-en-1-ol placed adjacent ($O^-\cdots C$ 1.770 Å) and with an $O{=}C\cdots O^-$ angle of approximately 105°. The model just prior to bond formation is illustrated in Figure 5a.

This suggests that in the first step the *tert*-butyl alcohol was initially sited above the Al atom, and that the prop-2-en-1-oxide anion remained associated with the LDH layer at the site of deprotonation, rather than occupying the site above the Al atom with the higher binding energy. The approaching methyl acetoacetate then occupied the Al site ready for the second stage of the reaction. Initially the reactants moved apart on the layer. The reaction only occurred when the methyl acetoacetate strongly interacted with the layer, directly implicating the MgAl LDH layer as the driving force in the reaction mechanism, rather than simply the suitable proximity and orientation of the reactant molecules.

In the final optimized structure (Figure 5b and Table 6) the alkoxide oxygen atom of the intermediate was located at a distance of 3.307 Å above the Al cation, nearly perpendicular (at an angle of 89.3°) to the *ab* plane. The alkoxide oxygen atom was located at the center of the three hydroxyl groups coordinated to the Al and interacted (H-bonds) with all three,

TABLE 6: Selected Calculated Bond Parameters for Intermediate Molecule (see Figure 1) Structure in Vacuo, for Comparison, and on LDH Layer[a]

bond	in vacuo model	step 2 in Figure 1
intermediate		
$C-O^-$	1.264 Å	1.291 Å
$C-OCH_3$	1.467 Å	1.424 Å
CH_2CHCH_2O-C	1.543 Å	1.568 Å
$C-CO^-$	1.594 Å	1.529 Å
CH_3-O	1.409 Å	1.410 Å
CH_2CHCH_2-O	1.405 Å	1.413 Å
$C-C-O^-$	114.16°	116.38°
CH_2CHCH_2O-C-C	105.88°	104.78°
CH_3O-C-C	103.66°	105.45°
interactions with LDH layer		
H-bond H3···O80		2.412 Å
H-bond H13···O80		2.327 Å
H-bond H13···O67		2.034 Å
H-bond H30···O67		1.829 Å
H-bond H40···O67		1.866 Å
Al···O67		3.307 Å
Al···O80		4.458 Å
ab-Al−O67		89.31°
ab-Al−O80		60.83°

[a] For numbering, see Figure 2.

with H-bond lengths in the range 1.829 Å to 2.034 Å. The prop-2-en-1-oxide fragment remained in its position astride the Mg atom adjacent to the Al, and is still H-bonded to the layer via the AlO−H and MgO−H H-bond donors as in section 3.2. The length of these H-bonds increased by as much as 30% to 2.327 and 2.412 Å, respectively, as a result of formation of the O−C bond.

The new bond between the prop-2-en-1-oxide fragment and the methyl acetoacetate was slightly longer at 1.568 Å than the in vacuo optimized length of 1.543 Å, mainly due to the continued interaction of the prop-2-en-1-oxy group oxygen atom with the LDH layer. H-bonding with the layer also resulted in an increased $C-O^-$ bond length of 1.291 Å (cf a value of 1.264 Å for the in vacuo structure). The carbonyl group decreased in bond order on reaction to form $C-O^-$ resulting in a change from the near planar sp^2 hybridized structure ($C{=}O$ 1.214 Å; $\angle O-C{=}O$ 123.7°(O−C═O angle)) found in the methyl acetoacetate to a tetrahedral sp^3 hybridized C in the intermediate ($\angle$MeO−C−C 105.4° (MeO−C−C angle)).

The optimized unit cell parameters, given in Table 2, were somewhat less than the model described in the previous section, but still larger than the optimized LDH layer without an anion. The *a* parameter was 9.569 Å and the *b* parameter 12.692 Å.

4.4. Intramolecular Rearrangement of Intermediate to Products. In this postulated step (step 3 in Figure 1) the intermediate generated in the prior reaction undergoes rearrangement back to a β-ketone ester, but with elimination of the methoxy substituent and retention of the prop-2-en-1-oxy group. The methoxy group is protonated while the *tert*-butyl alcohol is deprotonated, resulting in catalyst regeneration and the starting point of a further catalytic cycle.

It was initially conceived that the intermediate was protonated at the methoxy group oxygen atom by the *tert*-butyl alcohol, simultaneously forming the products and regenerating the catalyst. However, *t*-butoxide is a far better base than the ether oxygen and as such, despite the simulation of a number of possible interlayer configurations, this reaction was not observed. The methoxy oxygen is sterically hindered with respect to attack by the rest of the bulky intermediate molecule, except at one face or from above. An attempt was made to stabilize the *tert*-butyl alcohol oxygen atom by associating it with the face of

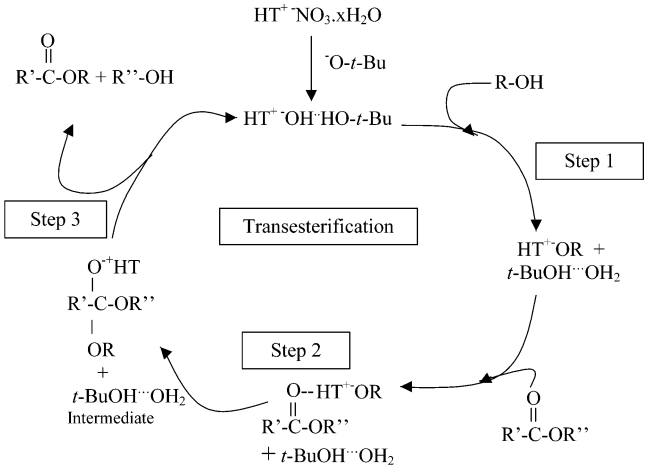

Figure 6. Scheme to show our proposed mechanism for the reaction studied by Choudary et al.[33] (see Figure 1), which is consistent with the simulations we have performed. HT refers to hydrotalcite, the naturally occurring mineral MgAl-carbonate LDH (LDHs are sometimes denoted HTLCs, hydrotalcite like compounds).

the MgAl layer opposing the intermediate, which necessitated the interlayer spacing be reduced to 10.50 Å. However, the bulky nature of the *tert*-butyl group restricted the proximity with which it was possible to place it adjacent to the methoxy oxygen group.

To achieve rearrangement of the intermediate it was necessary to include a water molecule in the simulation, thermal effects (i.e., perform an MD simulation at 363K) and also to decrease the interlayer spacing to 10.50 Å. Though water is invariably incorporated into the interlayer of LDH's during synthesis it was expected that the *t*-butoxide, a very strong base, would deprotonate any interlayer water, resulting in the formation of *tert*-butyl alcohol, and hydroxide anions as the charge balancing anion in the LDH. The hydroxide anions would then be displaced by excess *t*-butoxide *providing* that enough *t*-butoxide were utilized during exchange. The rearrangement of the intermediate with the water molecule present is described in the next section. We also propose a mechanism to account for the presence of the water molecules.

5. Results and Discussion: MgAl-Hydroxide LDH Catalyst

The presence of water in the interlayer region of the MgAl LDH suggests *t*-butoxide cannot be the charge-balancing anion. We postulate that the presence of water arises due to deprotonation of the prop-2-en-1-ol by a hydroxide anion, which was generated by reaction of the *t*-butoxide with interlayer water in the MgAl-nitrate LDH during preparation of the catalyst (see section 2). The catalyst is the MgAl-hydroxide LDH, with the polar *tert*-butyl alcohol molecule remaining in the interlayer. A proposed mechanism scheme, based on the mechanism of Choudary et al,[33] is described in Figure 6.

MgAl LDHs intercalated with hydroxide anions have been shown by Choudary et al. to be excellent solid base catalysts. In tests, a MgAl-hydroxide LDH formed by the rehydration method gave a reaction yield, for transesterification, of 77% after 12h, in comparison to the same reaction carried out with the MgAl *t*-butoxide LDH catalyst where a yield of 98% was reported after just 2h.[33]

In the rest of this section we describe this alternative method by which we have successfully simulated the entire catalytic cycle for the transesterification reaction using a MgAl-hydroxide LDH catalyst. Initially we describe the preparation of the MgAl-hydroxide LDH catalyst and then go on to outline the simulated reactions at each step of the proposed cycle in Figure 6.

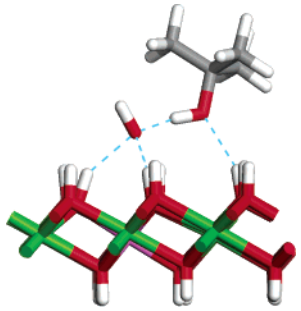

Figure 7. Optimized hydroxide LDH catalyst showing associated *tert*-butyl alcohol molecule and H-bonding (dashed lines). The color scheme is the same as that for Figure 2, with gray used for carbon and pale blue dashed lines indicating hydrogen bonding. Periodic boundary conditions are imposed in all three orthogonal space directions, with a vertical interlayer spacing of 16 Å.

TABLE 7: Selected Calculated Unit Cell and Bond Parameters for Optimized LDH Layers

parameter	optimized LDH layer	LDH catalyst (section 5.1)	step 1 in Figure 6 (section 5.2)	step 3 in Figure 6 (section 5.4)[a]
a	9.512 Å	9.578 Å	9.638 Å	9.426 Å
b	12.620 Å	12.684 Å	12.727 Å	12.568 Å
α	90.06°	90.41°	90.67°	90.00°
β	90.00°	89.62°	89.52°	90.00°
AlO−H13	0.969 Å	1.011 Å	0.975 Å	1.006 Å
AlO−H30	0.969 Å	0.989 Å	0.985 Å	0.985 Å
AlO−H40	0.969 Å	0.983 Å	0.983 Å	0.962 Å
Al−O1	1.890 Å	1.916 Å	1.903 Å	2.094 Å
Al−O4	1.902 Å	1.925 Å	1.920 Å	1.949 Å
Al−O7	1.892 Å	1.907 Å	1.907 Å	1.883 Å
Al···Mg (mean)	3.169 Å	3.159 Å	3.186 Å	3.099 Å
ab-AlO−H13	87.52°	72.27°	78.91°	71.12°
ab-AlO−H30	87.79°	71.76°	74.49°	71.16°
ab-AlO−H40	88.34°	77.26°	77.93°	73.36°
Mg16−O12Al	2.193 Å	2.135 Å	2.163 Å	2.063 Å
Mg46−O42	2.105 Å	2.108 Å	2.117 Å	2.093 Å
Mg46−O47	2.133 Å	2.165 Å	2.190 Å	2.204 Å
Mg46−O52	2.099 Å	2.091 Å	2.096 Å	2.291 Å
ab-MgO−H20	88.02°	85.88°	88.76°	76.84°
ab-MgO−H43	88.09°	85.57°	87.57°	59.82°

[a] MD simulation, after 164 fs simulation time.

5.1. Catalyst Formation. A model consisting of the optimized LDH layer, with one water molecule located above the Al atom, was minimized with respect to energy and an optimized *t*-butoxide molecule was introduced to a site located 4 Å perpendicular to a Mg atom adjacent to the Al atom in the LDH layer. The resulting model was minimized with respect to energy. Figure 7 shows the interlayer arrangement in the fully optimized model.

The water molecule was deprotonated by the *t*-butoxide, leaving a hydroxide anion triaxially coordinated, via H-bonds, to the three hydroxyl groups associated with the Al atom in the layer. Selected measured bond parameters for the LDH layer are given in Table 7. The *tert*-butyl alcohol molecule remained H-bonded to the hydroxyl anion at a distance of 1.564 Å, and also interacted with the LDH layer via a H-bond (2.361 Å) formed between the *tert*-butyl alcohol oxygen atom and a layer hydroxyl group.

The products, *tert*-butyl alcohol and a hydroxide anion, were observed to have moved toward each other, and were slightly displaced from their original starting positions. The *t*-butoxide oxygen atom moved to a point with an *ab*-Mg−HO*t*Bu angle (∠*ab*-Mg−HO*t*Bu) of 82.71° and a distance of 3.811 Å from

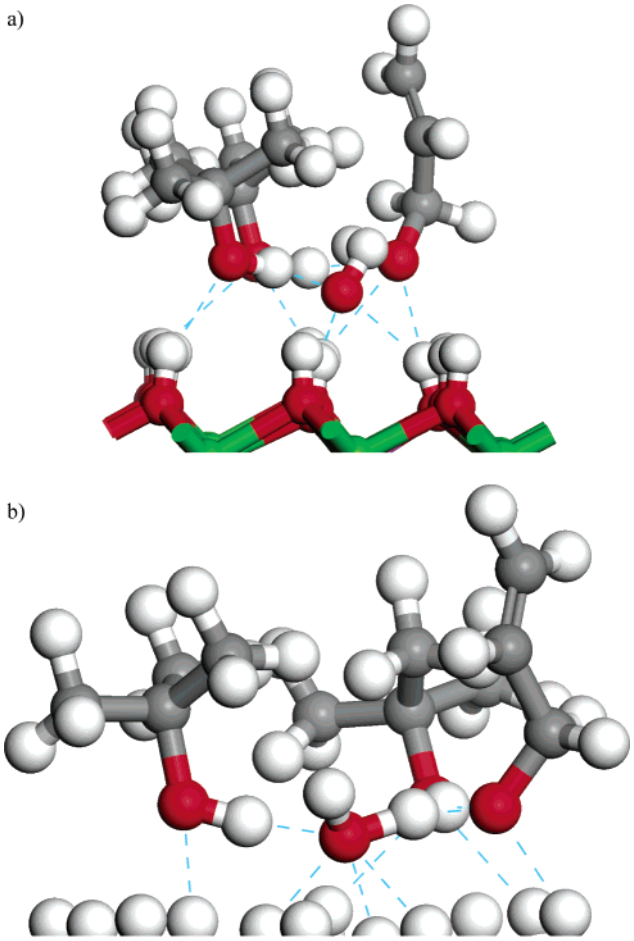

Figure 8. Stage 1 MD simulation showing (a) initial model showing the energy-minimized structure and (b) a closeup of the model after 77 fs of simulation showing the deprotonation of prop-2-en-1-ol. The color scheme is the same as that as for Figure 4.

the Mg atom it was initially located above. Similarly, the hydroxide oxygen atom in the energy-minimized structure was observed to be at an angle ∠*ab*-Al−HO of 85.81°, and at a distance of 3.269 Å to the Al atom in the layer.

The binding energies of a hydroxide anion, as well as water and nitrate molecules, sited above the Al atom on the LDH layer were calculated as described earlier and were found to be in the following order: OH^- > *t*-BuO^- > H_2O > $NO3^-$ (Table 5).

5.2. Reaction of Prop-2-en-1-ol on Catalyst. The optimized prop-2-en-1-ol reactant molecule was placed at various sites on the LDH layer of the optimized catalyst computed in the previous stage to form the starting point for the simulation of step 1 in Figure 6. No deprotonation of the prop-2-en-1-ol was observed upon optimization. Molecular dynamics simulations were then carried out on these optimized models for a time period of approximately 0.1ps. Proton transfer was not observed in the simulated systems.

Upon the addition of a second *tert*-butyl alcohol molecule to the system deprotonation of the prop-2-en-1-ol molecule now occurred during MD simulations at a simulated temperature of 363 K, as illustrated in Figure 8. Analysis of the binding energy of the hydroxide anion in the different models showed that introducing additional molecules led to a lowering of the hydroxide−LDH binding energy (Table 5).

We suggest that this is due to the "spectator" species partially stabilizing the positively charged LDH layer, resulting in a concomitant decrease in Coulombic attraction between the hydroxide anion and the layer. It should be noted that our model system is at best an approximation of reality; in the experimental process both substrate molecules are introduced simultaneously to the catalyst—conditions of too great a complexity to be readily modeled currently, which may result in far greater activation of the catalyst.

Table 7 gives the unit cell parameters and selected bond lengths and angles for the LDH layer in the optimized model that upon MD simulation resulted in a successful reaction. Analysis of the interlayer arrangement after deprotonation (75fs of elapsed MD simulation) shows that the water molecule has a 5-fold coordination, being triaxially coordinated to the hydroxyl groups at the Al site, with one H-bond to a *tert*-butyl alcohol molecule and another to the prop-2-en-1-oxide molecule. The H-bonds formed to the LDH layer were between 1.936 and 2.210 Å, and were approximately 10−15% longer than in the case of the hydroxide anion, indicating the reduced attraction between the layer and the neutral water molecule. The water molecule oxygen atom was observed to reside at a distance of 3.419 Å above the Al atom, with an ∠*ab*-Al−H_2O of 87.58°. The water molecule was observed to be asymmetric, as a result of interaction with the generated alkoxide anion, having one O−H bond of length 1.115 Å, and the other at 0.970 Å.

5.3. Reaction of Prop-2-en-1-oxide with Methyl Acetoacetate. This step in our proposed reaction mechanism (step 2, Figure 7) was considered to be essentially equivalent to that described in the analogous section for the original proposed mechanism (section 4.3). Though not included, the presence of the polar *tert*-butyl alcohol and water molecules within the interlayer is liable to facilitate the reaction by reducing the binding energy of the anion at the LDH layer face, as detailed in the previous section (section 5.2).

5.4. Intramolecular Rearrangement of Intermediate. This stage corresponds, in part, to step 3 in Figure 6. The water molecule acts as a Brønsted acid and is small enough to approach the sterically hindered methoxy group oxygen atom on the intermediate. To achieve a close proximity between the water molecule and the methoxy group oxygen atom it was necessary to reduce the interlayer spacing to 10.50 Å. Figure 9a illustrates the interlayer arrangement where reaction occurred after 159fs of molecular dynamics simulation at a simulated temperature of 363 K. The water molecule, itself polarized by the three Al-hydroxy groups in the adjacent layer and the *tert*-butyl alcohol, was small enough to approach the methoxy oxygen closely and polarize the C−O bond via hydrogen bonding to facilitate abstraction of the methoxy group. Selected bond measurements for the system at the step prior to and upon removal of the methoxy group are given in Table 8. It was observed that the methoxy group was generated prior to protonation of the methoxy oxygen and simultaneous deprotonation of the water molecule was not observed to occur. Unit cell parameters and selected bond parameters for the LDH MgAl layer are given in Table 7.

5.5. Regeneration of Catalyst. The methoxy group generated in the previous step was observed to abstract a proton from the water molecule present at the hydroxyl layer face, leaving a hydroxide anion to provide charge compensation for the positive site on the MgAl layer (Figure 9b) and thereby generating the catalyst described previously (section 5.1) and completing step 3 in our proposed mechanism shown in Figure 6. The hydroxide anion generated was not sufficiently basic in nature to abstract the alcohol proton from the *tert*-butyl alcohol molecule on the time scale of our simulations, though the *tert*-butyl alcohol remains associated via H-bonds to this hydroxide anion.

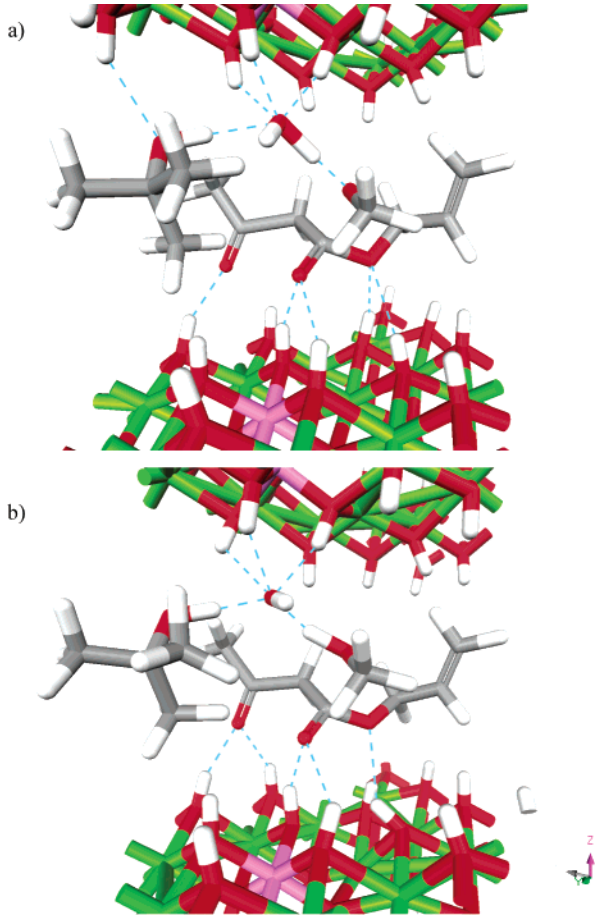

Figure 9. Stage 3 MD simulation: (a) model after 159 fs simulation showing rearrangement of intermediate and (b) model after 269 fs of simulation showing regeneration of basic catalyst site. The color scheme is the same as that for Figure 4.

TABLE 8: Selected Calculated Bond Parameters Prior to and upon Rearrangement of Intermediate Molecule (See Figure 6)

bond	prior to reaction	after reaction (see Figure 9)
intermediate		
C−O$^-$	1.271 Å	1.256 Å (C═O)
C−OCH$_3$	1.724 Å	
CH$_2$CHCH$_2$O−C	1.414 Å	1.424 Å
C−CO$^-$	1.547 Å	1.546 Å
CH$_3$−O	1.419 Å	1.425 Å
HO−H···O	1.189 Å	1.124 Å
C−C−O$^-$	111.37°	113.15°
CH$_2$CHCH$_2$O−C−C	116.40°	115.80°
CH$_3$O−C−C	103.73°	-
t-BuOH···OH$_2$	2.003 Å	1.965 Å
interactions with LDH layer		
H-bond AlO−H5···OH$_2$	1.773 Å	1.791 Å
H-bond AlO−H8···OH$_2$	2.323 Å	2.301 Å
H-bond AlO−H2···OH$_2$	1.770 Å	1.808 Å
H-bond H30···O$_{intermed}$[a]	2.211 Å	2.245 Å
H-bond H13···O$_{intermed}$	1.725 Å	1.725 Å
Al···OH$_2$	3.385 Å	3.382 Å
Al···O$_{intermed}$	3.490 Å	3.382 Å
ab-Al−OH$_2$	83.89°	83.66°
ab-Al−O$_{Intermed}$	72.27°	72.30°

[a] O$_{intermed}$ is the oxygen atom on the intermediate moiety that interacts with the Al site on the LDH layer. Prior to reaction O$_{intermed}$ is C−**O**$^-$, after reaction it is C═**O**.

This suggests that the catalytic properties of the *t*-butoxide MgAl LDHs are principally due to the hydroxide anions generated in situ within the gallery region by hydrolysis of interlayer water by the *t*-butoxide anion during the initial exchange reaction in preparing the *t*-butoxide MgAl-LDH catalyst.

6. Conclusions

Despite, or perhaps as a result of, the simplistic approach taken it has been possible, for the first time, to simulate the proposed steps of a model reaction mechanism within anionic clays by using ab initio calculations. Although, at this stage, it is not feasible to use these techniques to compute meaningful thermodynamic or kinetic parameters, it has been possible to investigate a variety of plausible orientations and interactions of molecules within this host−guest catalyst system and identify those that are indeed suitable to account for experimental observations.

In the system investigated here, it has been shown that certain parts of the reaction mechanism may be inherently robust; that is, they may occur within a wide range of interlayer arrangements, while other steps are far more sensitive to the relative orientation and interactions between the reactants. These latter steps may be considered to be the steps that control the overall rate of the reaction as they are statistically less favorable than the former.

Our study has highlighted the important role played by the Al sites, particularly the very active H-bond donor hydroxyl groups. There has long been uncertainty about whether the Al atom site has a higher charge than the surrounding layer, and consequently is more chemically active. In processes where H-bond interactions are dominant, such as in LDHs, an understanding of the behavior of the layer H atoms is paramount yet difficult to achieve experimentally due to the difficulty of resolving the H atom coordinates by conventional analytical techniques. Our simulations provide useful insight into these factors. Our findings suggest that an increase in the Al loading should provide more active sites at which reactions may occur. These results concur with the findings of Trave et al, who examined the electronic properties of MgAl−Cl LDHs and MgAl−OH LDHs using DFT methods in an attempt to elucidate the increased basic activity of the latter species.[29]

Our simulations have given insight into other factors that may be responsible for the excellent yields obtained by *t*-butoxide LDH catalysts, such as the bipolar nature of the material, and the ability of the 2-dimensional LDH structures to vary interlayer spacing when compared to the rigid 3-dimensional architecture of, for example, zeolites. By bipolar nature we refer to the fact that organo-LDHs consist of semirigid 2-dimensional sheets along the face of which exists a hydrophilic layer of hydroxyl groups, hydroxide anions and water molecules, and between these hydrophilic layers an organophilic layer (in this case *tert*-butyl molecules) resides. Organic substrates with polar functional groups intercalate so that the polar groups are orientated toward the LDH layer, mediating reactions through limiting possible reactant molecule alignments within the interlayer. The presence of neutral polar molecules at the LDH layer face acts to compensate the layer charge. This results in a decrease in binding energy of the anion and activation of the catalytic site.

The inability of the simulations of the proposed reaction to proceed without the presence of interlayer water molecules shows that the catalytic properties arise as a consequence of the bipolar nature of the *t*-butoxide LDH rather than the basic nature of the *t*-butoxide. Our simulations suggest the synthesized LDH is actually principally charge balanced by hydroxide anions, generated through reaction of interlayer water with

t-butoxide during the exchange process, and the resultant *tert*-butyl alcohol molecules are intercalated as polar, but neutral, entities. The reactivity is enhanced relative to the rehydrated calcined LDH catalyst[33] due to the presence of a hydrophobic interlayer region coupled with an increased interlayer spacing facilitating exchange of the organic substrate molecule.

These insights appear to be borne out to some extent by the experimental findings of Rao et al, who investigated the catalytic properties of calcined, and calcined-rehydrated MgAl LDHs on aldol condensation reactions. They reported that, despite the increased basicity of the calcined LDH, the less basic rehydrated catalyst performed better.[40] Choudary et al. also reported a lower yield for the transesterification reaction studied here using the more basic calcined MgAl catalyst than was observed for either the rehydrated or butoxide MgAl catalyst.[33] The simulation work of Trave et al., on anhydrous MgAl−OH LDHs, also illustrated the superior activity of the hydroxide intercalated LDH basic catalysts when compared to the chloride intercalated analogue.[29] We are currently investigating synthetic strategies to prepare MgAl-nitrate LDHs of varying Mg/Al ratio and with varying water content, to determine the effect that this has on the catalytic process.

Acknowledgment. The authors acknowledge the EPSRC and the Isaac Newton Trust for the funding of H.C.G., and Queen Mary, University of London and W. R. Grace & Co.-Conn. for funding S. Stackhouse. We thank the Cambridge Cranfield HPCF for providing access to CASTEP, HEFCE (U.K.) for funding our SGI Onyx2 computer, and the support of Accelrys and the CASTEP development group, in particular Phil Hasnip and Stewart Clarke.

References and Notes

(1) Newman, S. P.; Jones, W. *New J. Chem.* **1998**, *22*, 105−115.
(2) Carlino, S. *Chem. Br.* **1997**, *33*, 59−62.
(3) Cavani, F.; Trifiro, F.; Vaccari, A. *Catal. Today* **1991**, *11*, 173.
(4) Wilson, O. C.; Olorunyolemi, T.; Jaworski, A.; Borum, L.; Young, D.; Siriwat, A.; Dickens, E.; Oriakhi, C.; Lerner, M. *Appl. Clay Sci.* **1999**, *15*, 265−279.
(5) Choy, J. H.; Park, J. S.; Kwak, S. Y.; Jeong, Y. J.; Han, Y. S. *Mol. Cryst. Liquid Cryst.* **2000**, *341*, 1229−1233.
(6) Tronto, J.; Crepaldi, E. L.; Pavan, P. C.; De Paula, C. C.; Valim, J. B. *Mol. Cryst. Liq. Cryst.* **2001**, *356*, 227−237.
(7) Choudary, B. M.; Kantam, M. L.; Kavita, B.; Reddy, C. V.; Figueras, F. *Tetrahedron* **2000**, *56*, 9357−9364.
(8) Kantam, M. L.; Choudary, B. M.; Reddy, C. V.; Rao, K. K.; Figueras, F. *Chem. Commun.* **1998**, 1033−1034.
(9) Manju, G. N.; Gigi, M. C.; Anirudhan, T. S. *Ind. J. Chem. Technol.* **1999**, *6*, 134−141.
(10) Carja, G.; Nakamura, R.; Aida, T.; Niiyama, H. *Microporous Mesoporous Mater.* **2001**, *47*, 275−284.
(11) Weir, M. R.; Moore, J.; Kydd, R. A. *Chem. Mater.* **1997**, *9*, 1686−1690.
(12) Vaccari, A. *Catal. Today* **1998**, *41*, 53−71.
(13) Aramendia, M. A.; Borau, V.; Jimenez, C.; Marinas, J. M.; Ruiz, J. R.; Urbano, F. J. *Appl. Catal. A−Gen.* **2001**, *206*, 95−101.
(14) Kagunya, W.; Hassan, Z.; Jones, W. *Inorg. Chem.* **1996**, *35*, 5970−5974.
(15) Liu, Y.; Wang, X. Z.; Yang, X. G.; Wu, Y. *React. Kinet. Catal. Lett.* **1999**, *68*, 399−405.
(16) Constantino, V. R. L.; Pinnavaia, T. J. *Inorg. Chem.* **1995**, *34*, 883−892.
(17) Choudary, B. M.; Kantam, M. L.; Bharathi, B.; Reddy, C. V. *Synlett* **1998**, 1203−1204.
(18) Choudary, B. M.; Kantam, M. L.; Kavita, B. *Green Chem.* **1999**, *1*, 289−292.
(19) Choudary, B. M.; Kantam, M. L.; Kavita, B. *J. Mol. Catal. A−Chem.* **2001**, *169*, 193−197.
(20) Choudary, B. M.; Kantam, M. L.; Reddy, C. V.; Rao, K. K.; Figueras, F. *Green Chem.* **1999**, *1*, 187−189.
(21) Sels, B. F.; De Vos, D. E.; Jacobs, P. A. *Catal. Rev.−Sci. Eng.* **2001**, *43*, 443−488.
(22) Allman, R.; P., J. H. *Neues Jahrb. Mineral.−Monatsh.* **1969**, *12*, 544.
(23) Ennadi, A.; Legrouri, A.; De Roy, A.; Besse, J. P. *J. Mater. Chem.* **2000**, *10*, 2337−2341.
(24) Aicken, A. M.; Bell, I. S.; Coveney, P. V.; Jones, W. *Adv. Mater.* **1997**, *9*, 496-500.
(25) Wang, J. W.; Kalinichev, A. G.; Kirkpatrick, R. J.; Hou, X. Q. *Chem. Mater.* **2001**, *13*, 145−150.
(26) Newman, S. P.; Williams, S. J.; Coveney, P. V.; Jones, W. *J. Phys. Chem. B* **1998**, *102*, 6710−6719.
(27) Newman, S. P.; Greenwell, H. C.; Coveney, P. V.; Jones, W. In *Layered Double Hydroxides: Present and Future*; Rives, V., Ed.; Nova Science: New York, 2001.
(28) Newman, S. P.; Di Cristina, T.; Coveney, P. V.; Jones, W. *Langmuir* **2002**, *18*, 2933−2939.
(29) Trave, A.; Selloni, A.; Goursot, A.; Tichit, D.; Weber, J. *J. Phys. Chem. B* **2002**, *106*, 12291−12296.
(30) Stackhouse, S.; Coveney, P. V.; Sandre, E. *J. Am. Chem. Soc.* **2001**, *123*, 11764−11774.
(31) Segall, M. D.; Lindan, P. J. D.; Probert, M. J.; Pickard, C. J.; Hasnip, P. J.; Clark, S. J.; Payne, M. C. *J. Phys.−Condens. Matter* **2002**, *14*, 2717−2744.
(32) Gillan, M. J.; Lindan, P. J. D.; Kantorovich, L. N.; Bates, S. P. *Mineral. Mag.* **1998**, *62*, 669−685.
(33) Choudary, B. M.; Kantam, M. L.; Reddy, C. V.; Aranganathan, S.; Santhi, P. L.; Figueras, F. *J. Mol. Catal. A−Chem.* **2000**, *159*, 411−416.
(34) Choudary, B. M.; Kantam, M. L.; Kavita, B.; Reddy, C. V.; Rao, K. K.; Figueras, F. *Tetrahedron Lett.* **1998**, *39*, 3555−3558.
(35) Xu, Z. P.; Zeng, H. C. *J. Phys. Chem. B* **2001**, *105*, 1743−1749.
(36) Otera, J. *Chem. Rev.* **1993**, *93*, 1449−1470.
(37) Methcohn, O. *J. Chem. Soc., Chem. Commun.* **1986**, 695−697.
(38) Billman, J. H.; Smith, W. T., Jr.; Rendall, J. L. *J. Am. Chem. Soc.* **1947**, *69*, 2058.
(39) Rehberg, C. E.; Fisher, C. H. *J. Am. Chem. Soc.* **1944**, *66*, 1203.
(40) Rao, K. K.; Gravelle, M.; Valente, J. S.; Figueras, F. *J. Catal.* **1998**, *173*, 115−121.
(41) Zigan, F.; Rothbauer, R. *Neues Jahrb. Mineral. Monatsh.* **1967**, *4*, 137−143.
(42) Saalfeld, H.; Wedde, M. *Z. Kristallogr. Kristallogr.* **1974**, *139*, 129−155.
(43) Kariuki, B. M.; Valim, J. B.; Jones, W.; King, J. *Acta Crystallogr., Sect. C* **1994**, *50*, 1665−1667.
(44) Devita, A.; Gillan, M. J.; Lin, J. S.; Payne, M. C.; Stich, I.; Clarke, L. J. *Phys. Rev. B* **1992**, *46*, 12964−12973.
(45) Vanderbilt, D. *Phys. Rev. B* **1990**, *41*, 7892−7895.
(46) Perdew, J. P.; Zunger, A. *Phys. Rev. B* **1981**, *23*, 5048−5079.
(47) Perdew, J. P.; Chevary, J. A.; Vosko, S. H.; Jackson, K. A.; Pederson, M. R.; Singh, D. J.; Fiolhais, C. *Phys. Rev. B* **1992**, *46*, 6671−6687.
(48) Perdew, J. P.; Burke, K.; Ernzerhof, M. *Phys. Rev. Lett.* **1996**, *77*, 3865−3868.
(49) Penev, E.; Kratzer, P.; Scheffler, M. *J. Chem. Phys.* **1999**, *110*, 3986−3994.
(50) Gale, J. D.; Rohl, A. L.; Milman, V.; Warren, M. C. *J. Phys. Chem. B* **2001**, *105*, 10236−10242.
(51) Steininger, R.; Bilgram, J. H.; Gramlich, V.; Petter, W. *Z. Kristallogr.* **1989**, *187*, 1−13.
(52) Capaz, R. B.; Caldas, M. J. *J. Mol. Struct.* (*Theochem*) **1999**, *464*, 31−38.
(53) Purdy, A. P.; George, C. F. *Polyhedron* **1994**, *13*, 709−712.
(54) Schmid, G.; Lehr, J.; Polk, M.; Boese, R. *Angew. Chem., Int. Ed. Engl.* **1991**, *30*, 1015−1016.
(55) Davies, J. E.; Kopf, J.; Weiss, E. *Acta Crystallogr., Sect. B* **1982**, *38*, 2251−2253.